

# Hovering stochastic oscillations in self-organized critical systems

Osame Kinouchi<sup>1\*</sup>, Ludmila Brochini<sup>2</sup> Ariadne de Andrade Costa<sup>3</sup>,  
João Guilherme Ferreira Campos<sup>4</sup> & Mauro Copelli<sup>41</sup>

<sup>1</sup>Universidade de São Paulo, Departamento de Física-FFCLRP,  
Ribeirão Preto, Brazil

<sup>2</sup>Universidade de São Paulo, Instituto de Matemática e Estatística,  
São Paulo, Brazil

<sup>3</sup>Universidade de Campinas, Instituto de Computação, Campinas,  
Brazil

<sup>4</sup>Universidade Federal de Pernambuco, Departamento de Física,  
Recife, Brazil

December 14, 2024

## Abstract

In the last decade, several models with adaptive mechanisms (link deletion-creation, dynamical synapses, dynamical gains) have been proposed as examples of self-organized criticality (SOC). However, all these systems present hovering stochastic oscillations around the critical region and the origin of this behaviour is not clear. Here we make a linear stability analysis of the mean field fixed points of three adaptive SOC systems. We find that the fixed points correspond to barely stable spirals that turn out indifferent at criticality where a Neimark-Sacker bifurcation occurs. This near indifference means that, in real systems, finite-size fluctuations (as well as external noise) can excite both stochastic oscillations and avalanches. The coexistence of these two types of neuronal activity is an experimental prediction that differs from standard SOC models.

## 1 Introduction

Conservative self-organizing critical (SOC) systems are by now well understood in the framework of out of equilibrium absorbing phase transitions [1, 2, 3, 4]. But, since natural systems that present power law avalanches (earthquakes, forest fires, etc.) are dissipative in the bulk, compensation (drive) mechanisms have been proposed to make the models at least conservative on average. It

seems, however, that these mechanisms do not work so well: they lead the systems to present “dirty criticality”, in which the system hovers around the critical region with stochastic oscillations [5].

The literature reserves the acronym ASOC (adaptive SOC) to models that have an explicit dynamics in topology or network parameters (link deletion and creation, adaptive synapses, adaptive gains) [6, 7, 8, 9]. In the area of neuronal avalanches [10, 11, 12, 13], a well known ASOC system that presents hovering stochastic oscillations (HSO) is the Levina, Herrmann and Geisel (LHG) model [14, 15, 16] which uses continuous time integrate-and-fire neurons and dynamic synapses (short-term depression) inspired by the work of Tsodyks and Markram [17, 18]. After that, similar models have been studied, for example excitable cellular automata [19] with LHG synapses [20, 21] and discrete time stochastic neurons with dynamic neuronal gains [22, 23, 24].

The exact origin of HSO in ASOC systems remains unclear [5, 16, 23, 24]. Here, we examine some representative discrete time ASOC models at the mean-field (MF) level. We find that they evolve as 2-d MF maps whose fixed points are barely stable spirals very close to a Neimark-Sacker bifurcation, which defines the critical point. This makes these almost undamped spirals very sensitive to fluctuations that can induce and sustain the HSO in finite size systems.

This kind of stochastic oscillation is known in the literature [25, 26, 27, 28, 29] but, to produce them, one ordinarily needs to fine tune the system close to the bifurcation point. In contrast, for ASOC systems, there is a natural recovery time scale that self-organizes the system very close to the critical point, so that the coexistence of HSO and scale-invariant phenomena (e.g. avalanches) is robust [14, 16, 20, 21, 22, 23].

All these dissipative models are instances of self-organized quasi-criticality (SOqC), as defined by Bonachela *et al.* [5, 16]. Although these models show no exact criticality, they are very interesting because they can explain the coexistence of power law distributed neuronal avalanches, very large events (“dragon kings” [30, 31, 32]) and stochastic oscillations [23, 24]. Also, the adaptive mechanisms are biologically plausible and local (i.e. do not use global non-local information to tune the system toward the critical region as occurs in other models [33, 34]).

## 2 Network model with stochastic neurons

We start with a network model with  $i = 1, \dots, N$  discrete time stochastic neurons [35, 36, 37, 38, 39], as recently studied by Brochini *et al.* [22] and Costa *et al.* [23].

We define a binary firing indicator where  $X_i = 1$  means a spike and  $X_i = 0$  means silence of the  $i$ -th neuron. The neuron spikes with a firing probability function  $\Phi(V)$  that depends on a real valued variable  $V$  (the membrane potential). The firing function can be any general monotonically increasing function  $0 \leq \Phi(V) \leq 1$ . For mathematical convenience, we use the so-called rational

function [23]:

$$P(X = 1|V) = \Phi(V) = \frac{\Gamma V}{1 + \Gamma V} \Theta(V), \quad (1)$$

where  $\Gamma$  is the neuronal gain (the derivative  $d\Phi/dV$  for small  $V$ ) and  $\Theta$  is the step Heaviside function. This firing function is shown in Fig. 1a.

The membrane voltage evolves as:

$$V_i[t + 1] = \frac{1}{N} \sum_{j=1}^N W_{ij} X_j[t] \quad \text{if } X_i[t] = 0, \quad (2)$$

$$V_i[t + 1] = 0 \quad \text{if } X_i[t] = 1, \quad (3)$$

where  $W_{ij}$  are real valued synaptic weights (with  $W_{ii} = 0$ ) and the voltage is reset to zero after a firing in the previous time step. Since  $\Phi(0) = 0$ , this means that two consecutive fires are not allowed (the neuron has a refractory period).

In the MF approximation, we substitute  $X_i$  by its mean value  $\rho = \langle X_i \rangle$ , which is our order parameter (density of firing neurons or density of active sites). Then, equation (2) reads  $V[t + 1] = W\rho[t]$ , where  $W = \langle W_{ij} \rangle$ . From the definition of the firing function Eq. (1), we have:

$$\rho[t + 1] = \int \Phi(V) p(V; t + 1) dV, \quad (4)$$

where  $p(V; t + 1)$  is the voltage density at time  $t + 1$ . In this paper we are interested in the stability analysis of fixed points, so it suffices to obtain the map for  $\rho[t]$  close to stationarity. After a transient where all neurons spike at least one time, equations (2) and (3) develop a voltage density that has two Dirac peaks,  $p(V; t + 1) = \rho[t]\delta(V) + (1 - \rho[t])\delta(V - W\rho[t])$ . Inserting in equation (4), we finally get:

$$\rho[t + 1] = \frac{\Gamma W \rho[t](1 - \rho[t])}{1 + \Gamma W \rho[t]}. \quad (5)$$

The  $1 - \rho[t]$  fraction corresponds to the density of silent neurons in the previous time step. We call this the static model because  $W$  and  $\Gamma$  are fixed control parameters.

The order parameter  $\rho$  has two fixed points:  $\rho^0 = 0$ , which is stable for  $\Gamma W < 1$ , and

$$\rho^* = \frac{\Gamma W - 1}{2\Gamma W}, \quad (6)$$

which is stable for  $\Gamma W > 1$ . This means that  $\Gamma_c W_c = 1$  is a critical line of a continuous absorbing state transition (transcritical bifurcation), see Fig. 1b and 1c. If parameters are put at this critical line one observes well behaved power laws for avalanche sizes and durations with the mean-field exponents  $-3/2$  and 2 respectively [22]. However, such fine tuning should not be allowed for systems that intend to be self-organized to criticality.

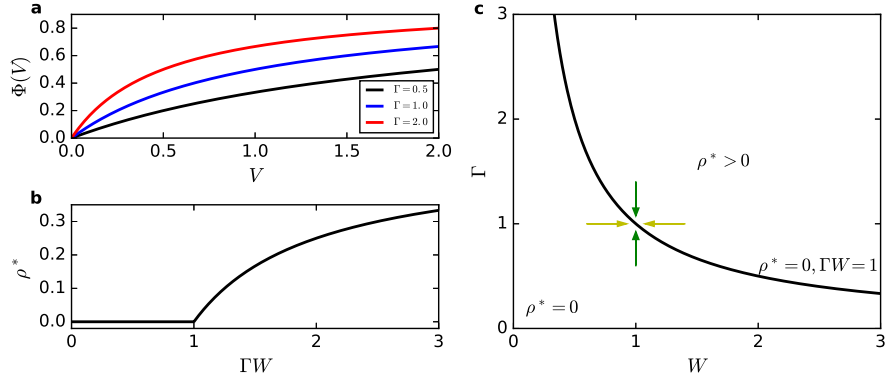


Figure 1: **Firing function  $\Phi(V)$ , firing density and phase diagram for the static model.** **a**, Rational firing function  $\Phi(V)$  for  $\Gamma = 0.5$  (bottom), 1.0 (middle) and 2.0 (top). **b**, Firing density  $\rho(\Gamma W)$ . The absorbing state  $\rho^0 = 0$  loses stability after  $\Gamma W > \Gamma_c W_c = 1$ . **c**, Phase diagram in the  $\Gamma \times W$  plane. ASOC can be done by adapting synapses (horizontal arrows) or adapting neuronal gains (vertical arrows) toward the critical line.

## 2.1 Stochastic neurons model with dynamic synapses

Adaptive SOC models try to turn the critical point (or at least the critical region) into an attractive fixed point of some homeostatic dynamics. For example, in the LHG model, the spike of the presynaptic neuron produces depression of the synapse, which recovers within some longer time scale [14, 16].

A model with stochastic neurons and LHG synapses uses the same equations (1–3) but the synapses change with time [22]:

$$W_{ij}[t+1] = W_{ij}[t] + \frac{\Delta t}{\tau} (A - W_{ij}[t]) - u W_{ij}[t] X_j[t]. \quad (7)$$

Here,  $\tau$  is the recovery time toward a baseline level  $A$  and  $0 < u < 1$  is the fraction of synaptic strength that is lost when the presynaptic neuron fires ( $X_j = 1$ ). From now, we always use  $\Delta t = 1$  ms, the typical width of a spike.

## 2.2 Stochastic neurons model with dynamic neuronal gains

Instead of adapting synapses toward the critical line  $W_c = 1/\Gamma$ , we can adapt the gains toward the critical condition  $\Gamma_c = 1/W$ , see Fig. 1c. This can be modeled as dynamic neuronal gains  $\Gamma_i[t]$  that decrease by a factor  $u$  if the neuron fires (diminishing the probability of subsequent firings) with a recovery time  $1/\tau$  toward a baseline level  $A$  [22]:

$$\Gamma_i[t+1] = \Gamma_i[t] + \frac{1}{\tau} (A - \Gamma_i[t]) - u \Gamma_i[t] X_i[t], \quad (8)$$

which is very similar to the LHG dynamics. Notice, however, that here we have only  $N$  equations for the neuronal gains instead of  $N(N-1)$  equations for dynamic synapses, which allows the simulation of much larger systems. Also, the neuronal gain depression occurs due to the firing of the neuron  $i$  (that is,  $X_i[t] = 1$ ) instead of the firing of the presynaptic neuron  $j$ . The biological location is also different: adaption of neuronal gains (firing rate adaptation) is a process that occurs at the axonal initial segment [40, 41] instead of synapses.

Like the LHG model, this dynamics has the inconvenient of having three parameters ( $\tau$ ,  $A$  and  $u$ ). Recently, we proposed a simpler dynamics with only one parameter [23, 24]:

$$\Gamma_i[t+1] = \Gamma_i[t] + \frac{1}{\tau}\Gamma_i[t] - \Gamma_i[t]X_i[t] = \left(1 + \frac{1}{\tau} - X_i[t]\right)\Gamma_i[t]. \quad (9)$$

Averaging over the sites, we obtain the MF 2-d map:

$$\rho[t+1] = \frac{\Gamma[t]W\rho[t](1-\rho[t])}{1+\Gamma[t]W\rho[t]}, \quad (10)$$

$$\Gamma[t+1] = \left(1 + \frac{1}{\tau} - \rho[t]\right)\Gamma[t]. \quad (11)$$

### 2.3 Stability analysis for stochastic neurons with simplified neuronal gains

This case with a single-parameter dynamics ( $\tau$ ) for the neuronal gains has the simplest analytic results, so it will be presented first and in more detail. For finite  $\tau$ ,  $\rho^0 = 0$  is no longer a solution, see equation (11), and the 2-d map has a single fixed point ( $\rho^*, \Gamma^*$ ):

$$\rho^* = \frac{1}{\tau}, \quad \Gamma^* = \frac{\Gamma_c}{1-2/\tau}, \quad (12)$$

where  $\Gamma_c = 1/W$ . The relation between  $\rho^*$  and  $\Gamma$  is:

$$\rho^* = \frac{\Gamma^*W - 1}{2\Gamma^*W} = \frac{\Gamma^* - \Gamma_c}{2\Gamma^*}, \quad (13)$$

which is similar to the expression for the phase transition in the static system, see equation (6). Here, however,  $\Gamma^*$  is no longer a parameter to be tuned but rather a fixed point to which the system dynamically converges. Notice that the critical point of the static model can be approximated for large  $\tau$ , with  $(\rho^*, \Gamma^*) \rightarrow (0, \Gamma_c)$ .

Performing a linear stability analysis of the fixed point (see Supplementary Information), we find that they correspond to stable spirals. The modulus of the complex eigenvalues is:

$$|\lambda^\pm| = \sqrt{1 - \frac{\tau+2}{\tau(\tau-1)}}. \quad (14)$$

For large  $\tau$ , the spiral is barely stable, that is,  $|\lambda^\pm| = 1 - O(1/\tau)$ , the Neimark-Sacker critical point occurring when  $|\lambda^\pm| = 1$ . For example, we have  $|\lambda^\pm| \approx 0.990$  for  $\tau = 100$ ,  $|\lambda^\pm| \approx 0.998$  for  $\tau = 500$  and  $|\lambda^\pm| \approx 0.999$  for  $\tau = 1,000$ . Since, due to biological motivations,  $\tau$  is in the interval of 100–1000 ms, we see that the spiral is at the border of losing its stability, that is, turning itself an indifferent fixed point very susceptible to fluctuations in the finite size real system.

## 2.4 Finite size simulations and the map with noise

The stability of the spiral is a result for the MF map that represents an infinite system without fluctuations. But fluctuations are present in any finite size system and one could say that these fluctuations can excite/drive the almost indifferent spiral, and sustain stochastic oscillations hovering around the fixed point.

Without loss of generality, we fix  $W = 1$  in the simulations. In Fig. 2a, we show the HSO for the firing density  $\rho[t]$  and average gain  $\Gamma[t]$  ( $\tau = 500$  and  $N = 100,000$ ). As observed in the original LHG model [16], the stochastic oscillations have a sawtooth profile with no constant amplitude or period. In Fig. 2b, we show the HSO in the phase plane  $\rho$  vs  $\Gamma$  for  $\tau = 100, 500$  and 1,000. The barely stable spirals of the MF map with the same  $\tau$  are shown in Fig. 2c. Finally, as a proof of concept, we add Gaussian noise to the  $\rho[t]$  variable in the MF map to simulate fluctuations (Fig. 2d). We see that the full system with  $N$  neurons and the 2-d map with noise present (qualitatively) the same stochastic oscillations. The amplitude and variance of the noise has been optimized to mimic the HSO.

For small amplitude (harmonic) oscillations, the frequency is given by (see Supplementary Information):

$$\omega = \arctan \frac{\sqrt{\tau + 2/\tau - 4}}{\tau - 2}. \quad (15)$$

The full oscillations are non-linear and their frequency depends on the amplitude, as seen in Fig. 2a. The oscillation period, also for small amplitudes, is given by  $T = 2\pi/\omega$ . Notice that, in the critical case, we have full critical slowing down:

$$\lim_{\tau \rightarrow \infty} \omega = \tau^{-1/2} \rightarrow 0, \quad \lim_{\tau \rightarrow \infty} T \rightarrow \infty. \quad (16)$$

This means that, exactly at the critical point, the 2-d map corresponds to a center without a period, and the HSO would be critical fluctuations in the  $\rho$  vs  $\Gamma$  plane. However, since for any physical system  $\tau$  is finite, the critical point is not observable.

## 2.5 Stochastic oscillations and avalanches

For large  $\tau$ , part of the HSO orbit occurs very close to the zero state  $\rho^0 = 0$ , see Fig. 2b. Due to finite-size fluctuations, the system frequently falls into this

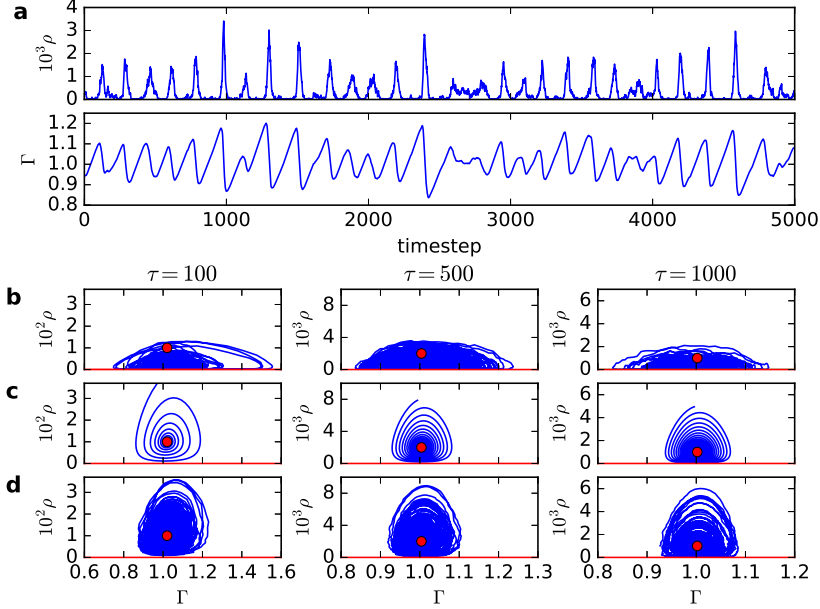


Figure 2: **Stochastic neurons network with simplified (one parameter) neuronal gain dynamics.** **a**, Stochastic oscillations for  $\rho[t]$  and  $\Gamma[t]$  ( $\tau = 500$ ,  $N = 100,000$  neurons). **b**, HSO in the  $\rho$  vs  $\Gamma$  phase plane for  $\tau = 100, 500$  and  $1,000$  ( $N = 100,000$ ). **c**, Damped spirals (transient) of the MF map with the same  $\tau$  values. **d**, HSO (stationary state) for the MF map with noise.

absorbing state. The orbits in phase space are interrupted. As in usual SOC simulations, we can define the size of an avalanche as the number  $S$  of firing events between such zero states. After a zero state, we force a neuron to fire, to continue the dynamics so that Fig. 2b is better understood as a series of patches (avalanches) terminating at  $\rho[t] = 0$ , not as a single orbit.

The presence of the HSO modifies the distribution of avalanche sizes  $P(S)$ , see Fig. 3. For small  $\tau$ ,  $\rho^*$  is higher and it is more difficult for the HSO to fall in the absorbing state. So, we see a bump for large events (long travels or loops in phase space). Increasing  $\tau$ , we approximate the Neimark-Sacker critical point and observe power laws with exponent  $-3/2$  similar to those produced in the transcritical static model. So, by using a different mechanism (Neimar-Sacker versus transcritical bifurcation), the ASOC model can reproduce experimental data about neuronal avalanches [10, 11, 12, 13]. It also predicts that avalanches can coexist with very large events [31, 32] and even stochastic neuronal oscillations. The  $P(S)$  distribution is not our main concern here and a more rigorous

finite size analysis can be found in previous papers [22, 23].

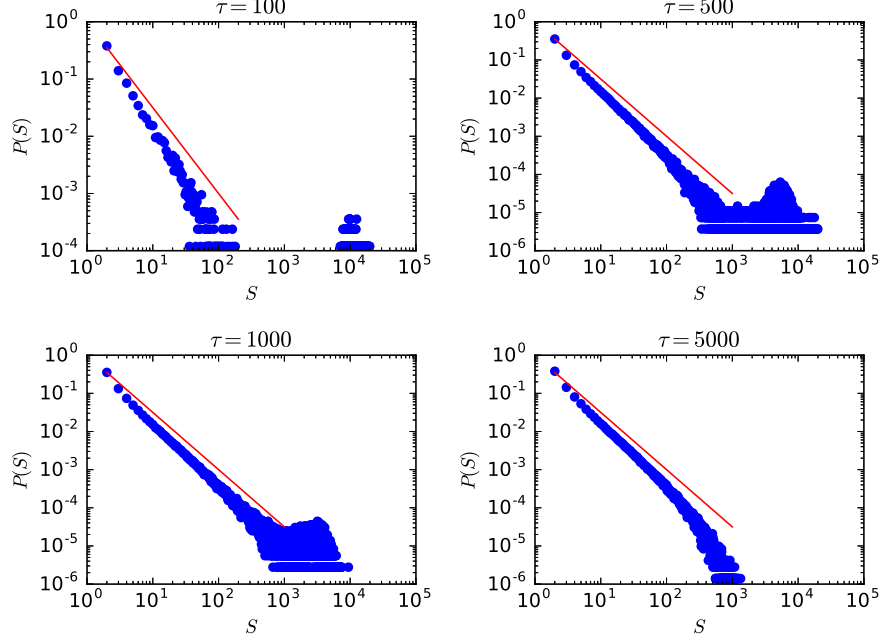


Figure 3: **Avalanche size distribution  $P(S)$  for the one parameter neuronal gains model.** From left to right,  $\tau = 100, 500, 1,000$  and  $5,000$ ; all plots have  $N = 100,000$ . The straight line corresponds to the exponent  $-3/2$ .

### Stochastic neurons with LHG dynamic gains

We now return to the case of dynamic gains with LHG dynamics, see equation (8). Without loss of generality, we use  $W = 1, \Gamma_c = 1/W = 1$ . The map is given by:

$$\rho[t+1] = \frac{\Gamma[t]\rho[t](1-\rho[t])}{1+\Gamma[t]\rho[t]}, \quad (17)$$

$$\Gamma[t+1] = \Gamma[t] + \frac{1}{\tau}(A - \Gamma[t]) - u\Gamma[t]\rho[t]. \quad (18)$$

The trivial absorbing fixed point is  $\rho^0 = 0, \Gamma = A$ , stable for  $A < 1$ , see Supplementary Material. For  $A > 1$ , we have a non-trivial fixed point given by:

$$\rho^* = \frac{A-1}{2A+\tau u}, \quad \Gamma^* = \frac{2A+\tau u}{2+\tau u}. \quad (19)$$

There is a relation between  $\rho^*$  and  $\Gamma^*$  that remembers the relation between the order parameter and the control parameter in the fixed model:

$$\rho^* = \frac{\Gamma^* - 1}{2\Gamma^*}, \quad (20)$$

valid for  $\Gamma^* > \Gamma_c = 1$ . Here, however,  $\Gamma^*$  is a self-organized variable, not a control parameter to be fine tuned.

We notice that to set by hand  $A = 1$ , pulling all gains toward  $\Gamma_i = 1$ , produces the critical point ( $\rho^* = 0, \Gamma^* = 1$ ). Nevertheless, this is a fine tuning that should not be allowed for SOC systems. We must use  $A > 1$ , and reach the critical region only by the large  $\tau$  limit:  $\rho^* \approx (A - 1)/\tau u$  and  $\Gamma^* \approx \Gamma_c + 2(A - 1)/\tau u$ .

Proceeding with the linear stability analysis, we obtain (see Supplementary Information):

$$\lambda^+ \lambda^- = \left(1 - \frac{1}{\tau}\right) \left(1 - \frac{2(A-1)}{A + u\tau + 1}\right) + \frac{u(A-1)^2}{(A + u\tau + 1)(2A + u\tau)}. \quad (21)$$

To first order in  $\tau$ , we have:

$$|\lambda^\pm| = \sqrt{\lambda^+ \lambda^-} = 1 - \frac{2(A-1) + u}{2u\tau} + O(\tau^{-2}), \quad (22)$$

which means that, for large  $\tau$ , the map is very close to the Neimark-Sacker critical point. As before, these almost undamped spirals can be excited by fluctuations, generating HSO in the finite-size systems.

For example, with the typical values  $A = 1.05$  and  $u = 0.1$  [20, 21], we have  $|\lambda^\pm| \approx 1 - 1/\tau$ , which gives  $|\lambda^\pm| \approx 0.990$  for  $\tau = 100$  and  $|\lambda^\pm| \approx 0.999$  for  $\tau = 1,000$ . In Fig. 4, we present the exact  $|\lambda^\pm|$ , the square root of equation (21), as a function of  $\tau$  for several values of  $A$  and  $u$ .

The frequency for harmonic oscillations is given by (see Supplementary Information):

$$\omega \simeq \sqrt{\frac{A-1}{\tau}} \quad (23)$$

The analysis of the stochastic neuron model with LHG synapses  $W_{ij}[t]$ , see equation (7), is very similar to the one above with LHG dynamic gains  $\Gamma_i[t]$ . The only difference is that we need to exchange  $\Gamma$  by  $W$ . The eigenvalue modulus is the same, so that LHG dynamic synapses also produce HSO. But, instead of presenting simulations in our complete graph system, which would involve  $N(N-1)$  dynamic equations for the synapses, we prefer to discuss the LHG synapses in another system well known in the literature. We will also examine how the HSO depend on the system size  $N$ .

### 3 Excitable cellular automata with LHG synapses

We now consider an ASOC version of a probabilistic cellular automata well studied in the literature [19, 42, 43, 44, 45]. It is a model for excitable media

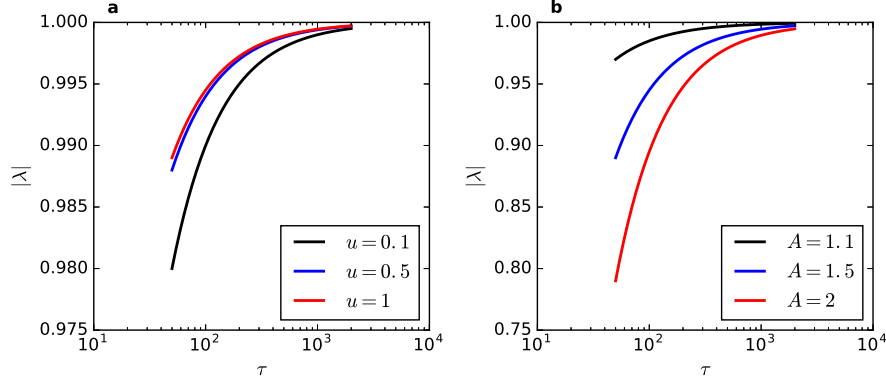


Figure 4: **Modulus  $|\lambda^\pm|$  as a function of  $\tau$  for several values of  $u$  and  $A$ .** **a**, From top to bottom,  $u = 0.1, 0.5$  and  $1$ , for  $A = 1.05$ . **b**, From top to bottom,  $A = 1.1, 1.5$  and  $A = 2$ , for  $u = 0.1$ .

and an interpretation in terms of neuronal networks is natural. Each site has  $n$  states,  $X = 0$  (silent),  $X = 1$  (firing),  $X = 2, \dots, n - 1$  (refractory). Here we will use  $n = 2$ .

Each neuron  $i = 1, \dots, N$  has  $K_i$  random neighbours (the average number in the network is  $K = \langle K_i \rangle$ ) coupled by probabilistic synapses  $P_{ij} \in [0, 1]$  (here we use  $K = 10$ , for implementation details see [19, 20, 21]). If the presynaptic neuron  $j$  fires at time  $t$ , with probability  $P_{ij}$  the postsynaptic neuron  $i$  fires at  $t + 1$ . The update is done in parallel, so the synapses are multiplicative, not additive like in the stochastic neuron model. All neurons that fire go deterministically to silence in the next step. Only neurons in the silent state can be induced to fire. Since  $1 - P_{ij}X_j$  is the probability that neighbour  $j$  does not induce the firing of neuron  $i$ , we can write the update rule as:

$$P(X_i[t + 1] = 1) = (1 - X_i[t]) \left[ 1 - \prod_j^{K_i} (1 - P_{ij}X_j) \right], \quad (24)$$

The control parameter of the static model is the branching ratio  $\sigma = K \langle P_{ij} \rangle$  and the critical value is  $\sigma_c = 1$ .

In the cellular automata (CA) model with LHG synapses, we have [20, 21]:

$$P_{ij}[t + 1] = P_{ij}[t] + \frac{1}{\tau} \left( \frac{A}{K} - P_{ij}[t] \right) - u P_{ij}[t] X_j[t]. \quad (25)$$

### 3.1 Mean field stability analysis

The 2-d MF map near the stationary state is:

$$\rho[t+1] = (1 - \rho[t]) \left[ 1 - \left( 1 - \frac{\sigma[t]\rho[t]}{K} \right)^K \right], \quad (26)$$

$$\sigma[t+1] = \sigma[t] + \frac{1}{\tau} (A - \sigma[t]) - u\sigma[t]\rho[t], \quad (27)$$

where in the second line we multiplied equation (25) by  $K$  and averaged over the synapses.

There is a trivial absorbing fixed point  $\rho^0 = 0, \sigma^0 = A$ , stable up to  $A = 1$ , see Supplementary Material. For  $A > 1$ , there exists a single fixed point given implicitly by:

$$\rho^* = (1 - \rho^*) \left[ 1 - \left( 1 - \frac{A\rho^*}{(1 + u\tau\rho^*)K} \right)^K \right], \quad (28)$$

$$\sigma^* = \frac{A}{1 + u\tau\rho^*}, \quad (29)$$

which we can solve numerically.

For this model we have numerical but not analytic results. However, we can find an approximate solution close to criticality, where  $\rho^*$  is small (see Supplementary Information). Expanding in powers of  $1/\tau$ , we get:

$$|\lambda^\pm| = 1 - \left( \frac{(A-1)(2K-1)}{2uK} + \frac{1}{2} \right) \frac{1}{\tau} + O(\tau^{-2}). \quad (30)$$

This confirms that the same scenario of barely stable spirals appears in the CA model.

This last result is particularly interesting. If we put  $K = N - 1$ , the CA network becomes a complete graph. Performing the limit  $N \rightarrow \infty$ , equation (30) gives:

$$|\lambda^\pm| = 1 - \frac{A-1+u/2}{u\tau} + O(\tau^{-2}), \quad (31)$$

which is identical to the  $|\lambda^\pm|$  value for the LHG stochastic neuron model, see equation (22).

Concerning the simulations, we must make a technical aside. In contrast to the static model [19], the relevant indicator of criticality here is no longer the branching ratio  $\sigma$ , but the principal eigenvalue  $\Lambda \neq \sigma$  of the synaptic matrix  $P_{ij}$ , with  $\Lambda_c = 1$  [42, 44]. This occurs because the synaptic dynamics creates correlations in the random neighbour network [21]. So, the MF analysis, where correlations are disregarded, does not furnish the exact  $\sigma[t]$  or  $\Lambda[t]$  of the CA model. But there exists an annealed version of the model in which  $\sigma[t] = \Lambda[t]$  and the MF analysis fully holds [20, 21]. In this version, when some neuron fires, the depressing term  $-uP_{ij}$  is applied to  $K$  synapses randomly chosen in the network. This is not biologically realistic, but destroys correlations and

restores the MF character of the model. Since all our analyses are done at the MF level, we prefer to present the simulation results using the annealed model. Concerning the HSO phenomenology, there are no qualitative differences between the annealed and the original CA model with LHG dynamics.

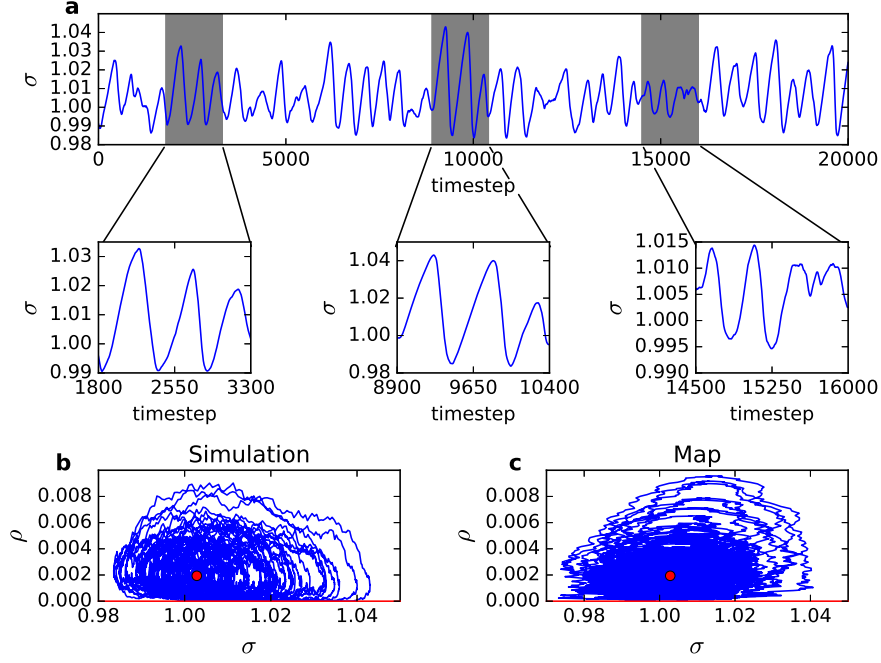


Figure 5: **Stochastic oscillations for the annealed CA model with LHG synapses.** **a**, The HSO for  $\sigma[t]$  has a sawtooth profile where large amplitudes have low frequency ( $N = 128,000$  neurons,  $\tau = 500$ ,  $A = 1.1$  and  $u = 0.1$ ). **b**, The HSO in the phase plane  $\rho$  vs  $\sigma$ . **c**, The MF map with Gaussian noise. The noise level has been adjusted to mimic the HSO. Transients have been discarded. The MF fixed point is the red dot.

The full stochastic oscillations in a system with  $N = 128,000$  neurons and  $\tau = 500$  can be seen in Fig. 5a and b. The angular frequency for small amplitude oscillations is given by equation (95) (see Supplementary Information) and we have  $\omega \simeq \sqrt{\frac{A-1}{\tau}}$  for large  $\tau$ , which is the same behavior found for the LHG dynamics with stochastic neurons, see equation (23).

The power spectrum of the time evolution of  $\rho$  and  $\sigma$  is shown in Fig. 6. The peak frequency gets closer to the theoretical  $\omega$  (vertical line) for larger system sizes because the oscillations have smaller amplitudes, going to the small oscillations limit.

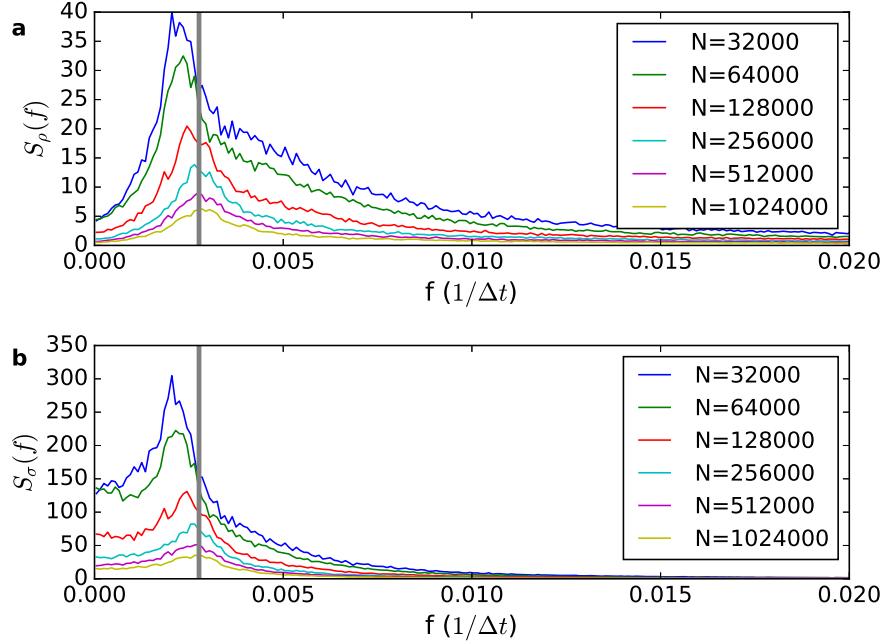


Figure 6: **Power spectrum of the time evolution of  $\rho$  and  $\sigma$  in the annealed CA model with LHG synapses.** **a** and **b**, power spectrum of the time evolution of  $\rho$  and  $\sigma$ , respectively, for different system sizes ( $\tau = 320$ ,  $A = 1.1$ ,  $u = 0, 1$ ). The vertical lines mark the theoretical value of the frequency of oscillations of the evolution of the MF map near the fixed point.

### 3.2 Dependence of HSO on system size

Now we ask if the HSO survive in the thermodynamic limit. In principle, given that fluctuations vanish in this limit, and we have always damped spirals for finite  $\tau$ , the HSO should also disappear when  $1/N \rightarrow 0$ . On the other hand, Bonachela *et al.* claimed that, in the LHG model, the width of the hovering behaviour basically does not change with  $N$  and is non-zero in the thermodynamic limit [16].

In Fig. 7, we measured the average  $\langle \sigma[t] \rangle$  and the standard deviation  $\Delta\sigma$  of the  $\sigma[t]$  time series of the annealed model. We used  $\tau = 320, 500, 1,000$  and  $2,000$  and systems sizes from  $N = 4,000$  to  $1,024,000$ . We interpret our findings as a  $\tau$  dependent crossover phenomenon due to a trade-off between the level of fluctuations (which depends on  $N$ ) and the level of dampening (which depends on  $\tau$ ): for a given  $\tau$ , a small  $N$  can produce sufficient fluctuations so that the HSO are sustained without change of  $\Delta\sigma$ . Nonetheless, for some  $N(\tau)$ , the fluctuations are not sufficient to compensate the dampening given by  $|\lambda^\pm| < 1$

and  $\Delta\sigma$  starts to decrease. The larger the  $\tau$ , the less damped is the spiral and the HSO survive without changing to a larger  $N$  (the plateau in Fig. 7b is more extended to the left).

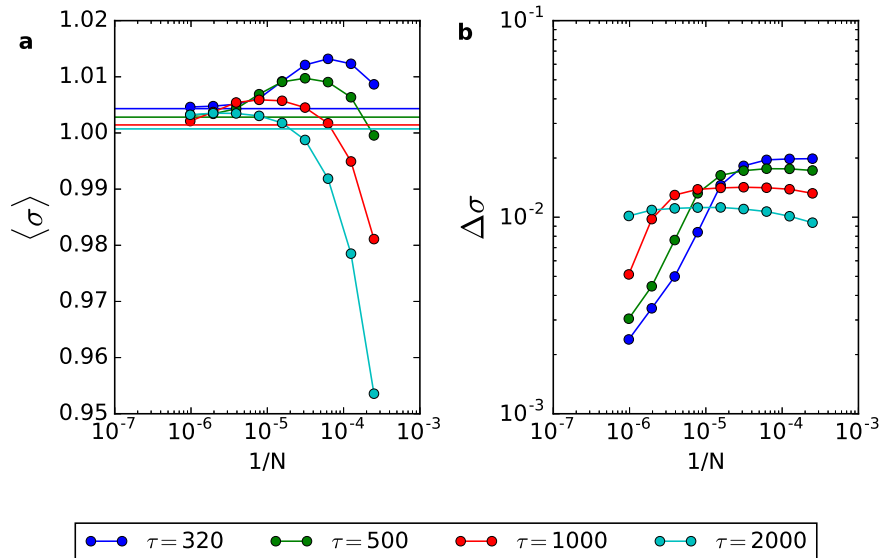


Figure 7: **Average and standard deviation of the HSO time series (CA model) as a function of  $1/N$ .** **a**, Average  $\langle\sigma[t]\rangle$  for different  $\tau$  values. Horizontal lines are the value of the fixed points  $\sigma^*$  given by equation (29). **b**, Standard deviation  $\Delta\sigma$  for different  $\tau$  values. Parameters are  $A = 1.1$  and  $u = 0.1$ . All measures are taken in a window of  $10^6$  time steps after discarding transients.

So, the conclusion is that, for any finite  $\tau$ , the HSO do not survive up to the thermodynamic limit, although they can be observed in very large systems. This is compatible with Fig. 6. We also see in Fig. 7a that  $\langle\sigma[t]\rangle \rightarrow \sigma^*$  for increasing  $N$ , so the system settles without variance at the MF fixed point  $(\rho^*, \sigma^*)$  in the infinite size limit.

We can reconcile our findings with those of the LHG model [14, 16] remembering an important technical detail: these authors used a synaptic dynamics with  $\tau = \tau_0 N$ , in an attempt to have the fixed point converging to the critical one in the thermodynamic limit (the same scaling is used in other models [9, 20]). In systems with  $\tau = O(N)$ , the fluctuations decay with  $N$  but, at the same time, the dampening controlled by  $\tau$  also decays with  $N$ . For this scaling  $\tau(N)$ , we can accept that the HSO survive in the thermodynamic limit. However, we already

emphasized that this is a non-biological and non-local scaling choice [21, 22, 23].

From a biological point of view, this discussion is not so relevant: although the finite-size fluctuations (called demographic noise in the literature [26, 27]) disappear for large  $N$ , external (environmental) noise, not included in the models, never vanishes in the thermodynamic limit. So, for practical purposes, the HSO would always be present. This external noise scenario corresponds better to our MF maps with noise (Fig. 2d and 5c).

## 4 Discussion and Conclusion

We now must stress what is new in our findings. Standard SOC models are related to static systems presenting an absorbing state phase transition [1, 2, 3, 4]. At the MF level, these static systems are described by a 1-d map  $\rho[t+1] = F(\rho[t])$  for the density of active sites, and the phase transition corresponds to a transcritical bifurcation where the critical point is an indifferent node. This indifferent equilibrium enables the occurrence of scale-invariant fluctuations in the  $\rho[t]$  variable, that is, scale-invariant avalanches but not stochastic oscillations (see however, HSO in some special sandpile models [46, 47]).

In ASOC, the original control parameter of the static system turns out an activity dependent variable leading to 2-d MF maps. We performed a MF fixed point stability analysis for three systems: 1) a stochastic neuronal model with one-parameter neuronal gain dynamics, 2) the same model with LHG gain dynamics, and 3) the CA model with LHG synapses. For the first one we obtained very simple and transparent analytic results; for the LHG dynamics we also got analytic, although more complex, results; finally, for the CA model, we were able to obtain a first order approximation for large recovery time  $\tau$ . Curiously, in the limit of  $K = (N - 1) \rightarrow \infty$  neighbours, the stochastic neuron model and the CA model have exactly the same first order leading term.

The complex eigenvalues have modulus  $|\lambda^\pm| \approx 1 - O(1/\tau)$  and, for large  $\tau$ , the fixed points are barely stable spirals, at the border of indifference. This means that, in finite size systems, fluctuations can excite and sustain the stochastic oscillations that hover around the fixed point, even for very large systems. We showed that this idea works by injecting noise in the MF maps and observing very similar HSO to the original models. To our knowledge, this stability analysis, although very simple, has never been done for ASOC systems. We believe that these results are generic and valid for the whole class of ASOC models, from networks with discrete deletion-recovery of links [7, 8, 9] to continuous depressing-recovering synapses [14, 16, 20, 21] dynamic neuronal gains [22, 23, 24]) and more complex synaptic mechanisms [33, 34]. This seems to be the case because all these systems present similar MF descriptions.

It must be clear that what is new here is not the stochastic oscillations based on damped spirals, since there is a whole literature in biosystems about that [25, 26, 27, 28, 29]. However, this literature corresponds to non-adaptive, static, models, in which the parameters must be fine tuned close to the relevant bifurcation. What is new in our work is the adaptive mechanism for producing

neuronal avalanches coexisting with large events and oscillations close to the critical Neimark-Sacker point. The tuning to the critical region is based on a large time scale  $\tau$  which is natural for the studied systems.

Very recently, di Santo *et al.* [48] studied a mesoscopic neural system with a Tsodyks-Markram dynamics (similar to the LHG model). They found that avalanches coexist with incipient oscillations at the border of a Hopf (synchronization) bifurcation, and propose that this mechanism, not the standard transcritical bifurcation, produces the neuronal avalanches. This conjecture is similar to ours (since a Neimark-Sacker bifurcation is the corresponding Hopf bifurcation for discrete time systems). The main difference is that they have a whole phase with oscillations above the critical point, so they have concerns about how to tune the system to criticality. In our case, we have a single phase of stable spirals with a limiting critical point close to where avalanches and HSO appear. The natural choice of large  $\tau$  tunes the system to the critical region.

So, in contrast to standard SOC, ASOC systems present stochastic oscillations that will not vanish in the thermodynamic limit if external (environmental) noise is present. But what seems to be a shortcoming for ASOC models could turn out to be an advantage. Since the adaptive dynamics with large  $\tau$  has good biological motivation, it is possible that HSO are experimentally observable, providing new physics beyond the standard model for SOC. The presence of the Neimark-Sacker bifurcation affects the distribution of avalanche sizes  $P(S)$ , creates dragon king events and large stochastic oscillations, and perhaps all this phenomenology could be measured [30, 49, 50]. In particular, our results are compatible with system-sized events (synchronized fires) recently observed in neuronal cultures [31, 32].

So, ASOC models have experimental predictions that differs from standard SOC based on a transcritical bifurcation (and also from criticality models based on Griffiths phases [51, 52]). We propose that the experimental detection of hovering stochastic oscillations and HSO based dragon-kings could be the next experimental challenge in the field of neuronal criticality.

Finally, we speculate that non-mean field models (square or cubic lattices) with dynamic gains and HSO could be applied to the modeling of dragon-kings and large quasiperiodic (characteristic) earthquakes that coexist with power-law distributions for the small events [53, 54]. This will be done in future work.

## Methods

**Numerical Calculations:** Numerical calculations were done by using MATLAB softwares. **Simulation procedures:** Simulation codes were made in Fortran90 and C++11.

## References

- [1] Dickman, R., Vespignani, A. & Zapperi, S. Self-organized criticality as an absorbing-state phase transition. *Phys. Rev. E* **57**, 5095 (1998).
- [2] Jensen, H. J. *Self-organized Criticality: Emergent Complex Behavior in Physical and Biological Systems* (Cambridge Univ. Press, Cambridge, UK, 1998).
- [3] Dickman, R., Muñoz, M. A., Vespignani, A. & Zapperi, S. Paths to self-organized criticality. *Braz. J. Phys.* **30**, 27–41 (2000).
- [4] Pruessner, G. *Self-organised Criticality: Theory, Models and Characterisation* (Cambridge Univ. Press, Cambridge, UK, 2012).
- [5] Bonachela, J. A. & Muñoz, M. A. Self-organization without conservation: true or just apparent scale-invariance? *J. Stat. Mech. - Theory Exp.* **2009**, P09009 (2009).
- [6] Bornholdt, S. & Rohlf, T. Topological evolution of dynamical networks: global criticality from local dynamics. *Phys. Rev. Lett.* **84**, 6114 (2000).
- [7] Meisel, C. & Gross, T. Adaptive self-organization in a realistic neural network model. *Phys. Rev. E* **80**, 061917 (2009).
- [8] Meisel, C., Storch, A., Hallmeyer-Elgner, S., Bullmore, E. & Gross, T. Failure of adaptive self-organized criticality during epileptic seizure attacks. *PLoS Comput. Biol.* **8**, e1002312 (2012).
- [9] Droste, F., Do, A.-L. & Gross, T. Analytical investigation of self-organized criticality in neural networks. *J. R. Soc. Interface* **10**, 20120558 (2013).
- [10] Beggs, J. M. & Plenz, D. Neuronal avalanches in neocortical circuits. *J. Neurosci.* **23**, 11167–11177 (2003).
- [11] Chialvo, D. R. Critical brain networks. *Physica A* **340**, 756–765 (2004).
- [12] Beggs, J. M. The criticality hypothesis: how local cortical networks might optimize information processing. *Philos. Trans. R. Soc. A* **366**, 329–343 (2008).
- [13] Chialvo, D. R. Emergent complex neural dynamics. *Nat. Phys.* **6**, 744–750 (2010).
- [14] Levina, A., Herrmann, J. M. & Geisel, T. Dynamical synapses causing self-organized criticality in neural networks. *Nat. Phys.* **3**, 857–860 (2007).
- [15] Levina, A., Herrmann, J. M. & Geisel, T. Phase transitions towards criticality in a neural system with adaptive interactions. *Phys. Rev. Lett.* **102**, 118110 (2009).

- [16] Bonachela, J. A., de Franciscis, S., Torres, J. J. & Muñoz, M. A. Self-organization without conservation: are neuronal avalanches generically critical? *J. Stat. Mech. - Theory Exp.* **2010**, P02015 (2010).
- [17] Tsodyks, M. & Markram, H. The neural code between neocortical pyramidal neurons depends on neurotransmitter release probability. *PNAS* **94**, 719–723 (1997).
- [18] Tsodyks, M., Pawelzik, K. & Markram, H. Neural networks with dynamic synapses. *Neural Networks* **10**, 821–835 (2006).
- [19] Kinouchi, O. & Copelli, M. Optimal dynamical range of excitable networks at criticality. *Nat. Phys.* **2**, 348–351 (2006).
- [20] Costa, A. A., Copelli, M. & Kinouchi, O. Can dynamical synapses produce true self-organized criticality? *J. Stat. Mech. - Theory Exp.* **2015**, P06004 (2015).
- [21] Campos, J. G. F., Costa, A. A., Copelli, M. & Kinouchi, O. Correlations induced by depressing synapses in critically self-organized networks with quenched dynamics. *Phys. Rev. E* **95**, 042303 (2017).
- [22] Brochini, L. *et al.* Phase transitions and self-organized criticality in networks of stochastic spiking neurons. *Sci. Rep.* **6**, 35831 (2016).
- [23] Costa, A. A., Brochini, L. & Kinouchi, O. Self-organized supercriticality and oscillations in networks of stochastic spiking neurons. *Entropy* **19**, 399 (2017).
- [24] Costa, A. A., Amon, M. J., Sporns, O. & Favela, L. H. Fractal analyses of networks of integrate-and-fire stochastic spiking neurons. In *International Workshop on Complex Networks*, 161–171 (Springer, 2018).
- [25] Nisbet, R. M. & Gurney, W. S. C. A simple mechanism for population cycles. *Nature* **263**, 319–320 (1976).
- [26] McKane, A. J. & Newman, T. J. Predator-prey cycles from resonant amplification of demographic stochasticity. *Phys. Rev. Lett.* **94**, 218102 (2005).
- [27] Risau-Gusman, S. & Abramson, G. Bounding the quality of stochastic oscillations in population models. *Eur. Phys. J. B* **60**, 515–520 (2007).
- [28] Wallace, E., Benayoun, M., Van Drongelen, W. & Cowan, J. D. Emergent oscillations in networks of stochastic spiking neurons. *PLoS One* **6**, e14804 (2011).
- [29] Baxendale, P. H. & Greenwood, P. E. Sustained oscillations for density dependent markov processes. *J. Math. Bio.* **63**, 433–457 (2011).
- [30] de Arcangelis, L. Are dragon-king neuronal avalanches dungeons for self-organized brain activity? *Eur. Phys. J. Spec. Top.* **205**, 243–257 (2012).

- [31] Orlandi, J. G., Soriano, J., Alvarez-Lacalle, E., Teller, S. & Casademunt, J. Noise focusing and the emergence of coherent activity in neuronal cultures. *Nat. Phys.* **9**, 582–590 (2013).
- [32] Yaghoubi, M. *et al.* Neuronal avalanche dynamics indicates different universality classes in neuronal cultures. *Sci. Rep.* **8**, 3417 (2018).
- [33] de Arcangelis, L., Perrone-Capano, C. & Herrmann, H. J. Self-organized criticality model for brain plasticity. *Phys. Rev. Lett.* **96**, 028107 (2006).
- [34] de Arcangelis, L. & Herrmann, H. Activity-dependent neuronal model on complex networks. *Front. Physiol.* **3**, 62 (2012).
- [35] Gerstner, W. Associative memory in a network of biological neurons. In *Advances in Neural Information Processing Systems*, 84–90 (1991).
- [36] Gerstner, W. & van Hemmen, J. L. Associative memory in a network of ‘spiking’ neurons. *Network: Comput. Neural Syst.* **3**, 139–164 (1992).
- [37] Gerstner, W. & Kistler, W. M. *Spiking Neuron Models: Single Neurons, Populations, Plasticity* (Cambridge Univ. Press, 2002).
- [38] Galves, A. & Löcherbach, E. Infinite systems of interacting chains with memory of variable length — a stochastic model for biological neural nets. *J. Stat. Phys.* **151**, 896–921 (2013).
- [39] Larremore, D. B., Shew, W. L., Ott, E., Sorrentino, F. & Restrepo, J. G. Inhibition causes ceaseless dynamics in networks of excitable nodes. *Phys. Rev. Lett.* **112**, 138103 (2014).
- [40] Kole, M. H. P. & Stuart, G. J. Signal processing in the axon initial segment. *Neuron* **73**, 235–247 (2012).
- [41] Pozzorini, C., Naud, R., Mensi, S. & Gerstner, W. Temporal whitening by power-law adaptation in neocortical neurons. *Nature neuroscience* **16**, 942 (2013).
- [42] Larremore, D. B., Shew, W. L. & Restrepo, J. G. Predicting criticality and dynamic range in complex networks: effects of topology. *Phys. Rev. Lett.* **106**, 058101 (2011).
- [43] Mosqueiro, T. S. & Maia, L. P. Optimal channel efficiency in a sensory network. *Phys. Rev. E* **88**, 012712 (2013).
- [44] Wang, C.-Y., Wu, Z.-X. & Chen, M. Z. Q. Approximate-master-equation approach for the kinouchi-copelli neural model on networks. *Phys. Rev. E* **95**, 012310 (2017).
- [45] Zhang, R. & Pei, S. Dynamic range maximization in excitable networks. *Chaos* **28**, 013103 (2018).

- [46] di Santo, S., Burioni, R., Vezzani, A. & Muñoz, M. A. Self-organized bistability associated with first-order phase transitions. *Physical review letters* **116**, 240601 (2016).
- [47] Saeedi, A., Jannesari, M., Gharibzadeh, S. & Bakouie, F. Coexistence of stochastic oscillations and self-organized criticality in a neuronal network: Sandpile model application. *Neural computation* **30**, 1132–1149 (2018).
- [48] di Santo, S., Villegas, P., Burioni, R. & Muñoz, M. A. Landau–ginzburg theory of cortex dynamics: Scale-free avalanches emerge at the edge of synchronization. *PNAS* **115**, E1356–E1365 (2018).
- [49] Poil, S.-S., van Ooyen, A. & Linkenkaer-Hansen, K. Avalanche dynamics of human brain oscillations: relation to critical branching processes and temporal correlations. *Hum. Brain Mapp.* **29**, 770–777 (2008).
- [50] Poil, S.-S., Hardstone, R., Mansvelder, H. D. & Linkenkaer-Hansen, K. Critical-state dynamics of avalanches and oscillations jointly emerge from balanced excitation/inhibition in neuronal networks. *J. Neurosci.* **32**, 9817–9823 (2012).
- [51] Moretti, P. & Muñoz, M. A. Griffiths phases and the stretching of criticality in brain networks. *Nat. Commun.* **4**, 2521 (2013).
- [52] Girardi-Schappo, M., Bortolotto, G. S., Gonsalves, J. J., Pinto, L. T. & Tragtenberg, M. H. R. Griffiths phase and long-range correlations in a biologically motivated visual cortex model. *Sci. Rep.* **6**, 29561 (2016).
- [53] Carlson, J. M. Time intervals between characteristic earthquakes and correlations with smaller events: An analysis based on a mechanical model of a fault. *J. Geophys. Res.* **96**, 4255–4267 (1991).
- [54] Wesnousky, S. G. The gutenbergrichter or characteristic earthquake distribution, which is it? *B. Seismol. Soc. Am.* **84**, 1940–1959 (1994).

## Acknowledgements

This article was produced as part of the activities of FAPESP Research, Innovation and Dissemination Center for Neuromathematics (Grant No. 2013/07699-0, S. Paulo Research Foundation). We acknowledge financial support from CAPES, CNPq, FACEPE, and Center for Natural and Artificial Information Processing Systems (CNAIPS)-USP. LB thanks FAPESP (Grant No. 2016/24676-1). AAC thanks FAPESP (Grants No. 2016/00430-3 and No. 2016/20945-8).

## Author contributions

AAC and JGFC performed the simulations and prepared all the figures. JGFC, LB, MC and OK made the analytic calculations. All authors contributed to the writing of the manuscript.

## Competing interests

The authors declare that they have no competing financial interests.

## Supplementary Information

### Stability analysis of the stochastic neuron model with one parameter ( $\tau$ ) gain dynamics

The MF map is:

$$\rho[t+1] = \frac{\Gamma[t]W\rho[t](1-\rho[t])}{1+\Gamma[t]W\rho[t]} = F(\rho[t], \Gamma[t]), \quad (32)$$

$$\Gamma[t+1] = \left(1 + \frac{1}{\tau} - \rho[t]\right) \Gamma[t] = G(\rho[t], \Gamma[t]). \quad (33)$$

Notice that  $(\rho^0 = 0, \Gamma)$  is not a fixed point. The single fixed point is:

$$\rho^* = \frac{1}{\tau}, \quad \Gamma^* = \frac{\Gamma_c}{1 - 2/\tau}. \quad (34)$$

To perform the fixed point stability analysis we calculate partial derivatives evaluated at the fixed point (denoted by  $]$ ):

$$a = \left. \frac{\partial F}{\partial \rho} \right]_* = \frac{\Gamma^*W - 2\Gamma^*W\rho^* - (\Gamma^*W\rho^*)^2}{[1 + \Gamma^*W\rho^*]^2} = \frac{\tau - 3}{\tau - 1}, \quad (35)$$

$$b = \left. \frac{\partial F}{\partial \Gamma} \right]_* = \frac{W\rho^*(1 - \rho^*)}{[1 + \Gamma^*W\rho^*]^2} = \frac{W(\tau - 2)^2}{\tau^2(\tau - 1)}, \quad (36)$$

$$c = \left. \frac{\partial G}{\partial \rho} \right]_* = -\Gamma^* = -\frac{\tau}{W(\tau - 2)}, \quad (37)$$

$$d = \left. \frac{\partial G}{\partial \Gamma} \right]_* = 1 + 1/\tau - \rho^* = 1. \quad (38)$$

The eigenvalues of the system Jacobian matrix at the fixed point  $(\rho^*, \Gamma^*)$  are determined by

$$\det(J - \lambda I) = (a - \lambda)(d - \lambda) - bc = 0. \quad (39)$$

So, the characteristic equation is:

$$\lambda^2 - \left[ \left( \frac{\tau - 3}{\tau - 1} \right) + 1 \right] \lambda + \frac{\tau - 3}{\tau - 1} + \frac{\tau - 2}{\tau(\tau - 1)} = 0. \quad (40)$$

That can be written as:

$$(\tau - 1)\tau\lambda^2 - (2\tau^2 - 4\tau)\lambda + \tau^2 - 2\tau - 2 = 0, \quad (41)$$

with solutions:

$$\lambda^\pm = \frac{\tau^2 - 2\tau \pm \sqrt{\Delta}}{\tau(\tau - 1)}, \quad (42)$$

$$\Delta = (\tau^2 - 2\tau)^2 - \tau(\tau - 1)(\tau^2 - 2\tau - 2) \quad (43)$$

This equation has no meaning for  $\tau < 2$  since this would give  $\rho^* = 1/\tau > 1/2$ . When  $2 < \tau < 2 + \sqrt{2}$  we have  $\Delta > 0$ ,  $\lambda$  real and  $|\lambda| < 1$ , that is, the fixed point  $(\rho^*, \Gamma^*)$  is a stable node. However, when  $\tau > 2 + \sqrt{2} = 3.4142\dots$ , we have  $\Delta < 1$  and two complex roots  $\lambda^\pm$  with  $|\lambda| = \sqrt{\lambda^+\lambda^-} < 1$ , that is, we have a stable spiral with:

$$\lambda^\pm = \frac{\tau^2 - 2\tau \pm i\sqrt{-\Delta}}{\tau(\tau - 1)}, \quad (44)$$

$$|\lambda^\pm| = \sqrt{\lambda^+\lambda^-} = \sqrt{\frac{\tau^2 - 2\tau - 2}{\tau(\tau - 1)}} = \sqrt{1 - \frac{\tau + 2}{\tau(\tau - 1)}}, \quad (45)$$

which leads to equation (14).

For small amplitude (harmonic) oscillations, the frequency is given by the angle of the eigenvalues written in polar coordinates. We can write it in terms of the determinant  $D$  and trace  $T$  of the Jacobian matrix  $J$  as

$$\omega \equiv |\omega^\pm| = \arctan \sqrt{\frac{4D}{T^2} - 1} = \arctan \frac{\sqrt{\tau + 2/\tau - 4}}{\tau - 2} \quad (46)$$

When  $\tau \rightarrow \infty$ ,

$$\omega \simeq \sqrt{\frac{1}{\tau}} \quad (47)$$

## Stability analysis of the stochastic neuron model with LHG gain dynamics

The MF map is given by:

$$\rho[t + 1] = \frac{\Gamma[t]\rho[t](1 - \rho[t])}{1 + \Gamma[t]\rho[t]} = F(\rho[t], \Gamma[t]), \quad (48)$$

$$\Gamma[t + 1] = \Gamma[t] + \frac{1}{\tau}(A - \Gamma[t]) - u\Gamma[t]\rho[t] = G(\rho[t], \Gamma[t]). \quad (49)$$

We have two fixed points. The absorbing state fixed point:

$$\rho^0 = 0 \quad \Gamma^0 = A, \quad (50)$$

and the non trivial fixed point  $(\rho^*, \Gamma^*)$ :

$$\rho^* = \frac{A-1}{2A+\tau u}, \quad \Gamma^* = \frac{2A+\tau u}{2+\tau u}. \quad (51)$$

Partial derivatives of  $F$  and  $G$  with respect to  $\rho$  and  $\Gamma$  are:

$$\frac{\partial F(\rho, \Gamma)}{\partial \rho} = -\frac{\Gamma(2\rho + \rho^2\Gamma - 1)}{(\rho\Gamma + 1)^2}, \quad (52)$$

$$\frac{\partial F(\rho, \Gamma)}{\partial \Gamma} = -\frac{(\rho-1)\rho}{(\rho\Gamma + 1)^2}, \quad (53)$$

$$\frac{\partial G(\rho, \Gamma)}{\partial \rho} = -\Gamma u, \quad (54)$$

$$\frac{\partial G(\rho, \Gamma)}{\partial \Gamma} = -\frac{1}{\tau} - u\rho + 1. \quad (55)$$

Evaluating at the trivial fixed point, we get:

$$a = \left. \frac{\partial F}{\partial \rho} \right|_0 = \Gamma = A, \quad (56)$$

$$b = \left. \frac{\partial F}{\partial \Gamma} \right|_0 = 0, \quad (57)$$

$$c = \left. \frac{\partial G}{\partial \rho} \right|_0 = -u\Gamma = -uA, \quad (58)$$

$$d = \left. \frac{\partial G}{\partial \Gamma} \right|_0 = 1 - \frac{1}{\tau}. \quad (59)$$

The eigenvalues are found from  $(a - \lambda)(d - \lambda) - bc = 0$ , or:

$$(A - \lambda)(1 - 1/\tau - \lambda) = 0, \quad (60)$$

$$\lambda^2 - (A + 1 - 1/\tau)\lambda + (1 - 1/\tau)A = 0, \quad (61)$$

with solution:

$$\lambda^\pm = \frac{(A + 1 - 1/\tau) \pm \sqrt{\Delta}}{2}, \quad (62)$$

$$\Delta = (A + 1 - 1/\tau)^2 - 4(1 - 1/\tau)A = [A - (1 - 1/\tau)]^2. \quad (63)$$

Notice that  $\Delta \geq 0$  so the eigenvalues are always real: the fixed point is an attractive or repulsive node. The final solution of Eq. 62 is:

$$\lambda^+ = A, \quad (64)$$

$$\lambda^- = 1 - 1/\tau. \quad (65)$$

This means that the fixed point  $(\rho^0 = 0, \Gamma^0 = A)$  is stable for  $\lambda^+ = A < 1$ . The critical point is  $A = 1$ .

This analysis show that we can have a subcritical state  $(0, A)$ , an attractive node, if we use  $A < 1$ . On the other hand, if we use  $A > 0$ , the absorbing state looses its stability and the non trivial fixed point  $(\rho^*, \Gamma^*)$  is the unique stable solution. For  $A = 1$ , the point  $(\rho^0 = 0, \Gamma^0 = 1)$  is an indifferent node.

Evaluating the derivatives at the non trivial fixed point, we get:

$$\left. \frac{\partial F}{\partial \rho} \right]_* = \frac{3 - A + u\tau}{A + u\tau + 1}, \quad (66)$$

$$\left. \frac{\partial F}{\partial \Gamma} \right]_* = \frac{(A - 1)(2 + u\tau)^2}{(A + u\tau + 1)(2A + u\tau)^2}, \quad (67)$$

$$\left. \frac{\partial G}{\partial \rho} \right]_* = -\frac{u(2A + u\tau)}{2 + u\tau}, \quad (68)$$

$$\left. \frac{\partial G}{\partial \Gamma} \right]_* = 1 - \frac{1}{\tau} - \frac{u(A - 1)}{2A + u\tau}, \quad (69)$$

As before, the eigenvalues of the Jacobian matrix at the fixed point  $(\rho^*, \Gamma^*)$  are determined by equation (39). After some algebra, we get:

$$\begin{aligned} |\lambda^+ \lambda^-| &= ad - bc \\ &= \frac{(1 - 1/\tau - \frac{u(A-1)}{2A+u\tau})(3 - A + u\tau)}{(A + u\tau + 1)} + \frac{u(2 + u\tau)(A - 1)}{(2A + u\tau)(A + u\tau + 1)}, \\ &= \left(1 - \frac{1}{\tau}\right) \left(1 - \frac{2(A - 1)}{A + u\tau + 1}\right) + \frac{u(A - 1)^2}{(A + u\tau + 1)(2A + u\tau)}. \end{aligned} \quad (70)$$

For large  $\tau$ , we have:

$$|\lambda^\pm| = \sqrt{\lambda^+ \lambda^-} = 1 - \frac{2(A - 1) + u}{2u\tau} + O(\tau^{-2}), \quad (71)$$

which means that, for large  $\tau$ , the map is very close to a Neimark-Sacker critical point. As before, the barely stable spirals can be excited by fluctuations, generating the HSO.

The frequency for harmonic oscillations is:

$$\omega \equiv |\omega^\pm| = \arctan \sqrt{\frac{4D}{T^2} - 1}. \quad (72)$$

Where D and T are respectively the determinant and trace of the Jacobian matrix. When  $\tau \rightarrow \infty$ ,

$$\omega \simeq \sqrt{\frac{A - 1}{\tau}} \quad (73)$$

which is consistent with equation (47) for the case with one parameter in gain dynamics.

## Stability analysis of the Cellular Automata model with LHG synapses

The 2-d MF map near the stationary state is:

$$\rho[t+1] = (1 - \rho[t]) \left[ 1 - \left( 1 - \frac{\sigma[t]\rho[t]}{K} \right)^K \right] = F(\rho[t], \sigma[t]), \quad (74)$$

$$\sigma[t+1] = \sigma[t] + \frac{1}{\tau} (A - \sigma[t]) - u\sigma[t]\rho[t] = G(\rho[t], \sigma[t]), \quad (75)$$

where in the second line we multiplied equation (25) by  $K$  and averaged over the synapses. As before, the stability of the map is given by the eigenvalues of the Jacobian matrix  $J(\rho, \sigma)$  at the fixed points. The matrix elements are:

$$\left. \frac{\partial F}{\partial \rho} \right] = \left[ \left( 1 - \frac{\sigma\rho}{K} \right)^K - 1 \right] + (1 - \rho)\sigma \left( 1 - \frac{\sigma\rho}{K} \right)^{K-1}, \quad (76)$$

$$\left. \frac{\partial F}{\partial \sigma} \right] = (1 - \rho)\rho \left( 1 - \frac{\rho\sigma}{K} \right)^{K-1}, \quad (77)$$

$$\left. \frac{\partial G}{\partial \rho} \right] = -u\sigma, \quad (78)$$

$$\left. \frac{\partial G}{\partial \sigma} \right] = 1 - \frac{1}{\tau} - u\rho. \quad (79)$$

Thus, we can plug in the solutions of equations (28) and (29) in equations (76-79) and find the eigenvalues of  $J(\rho, \sigma)$ .

Similarly to the previous model, the MF map of the CA with LHG synapses has two fixed points. The first one is the absorbing state fixed point and is given by

$$\rho^0 = 0 \quad \sigma^0 = A. \quad (80)$$

The second one is nontrivial and must be solved numerically.

We can compute the elements of the Jacobian matrix at the absorbing state fixed point

$$\left. \frac{\partial F}{\partial \rho} \right]_0 = A, \quad (81)$$

$$\left. \frac{\partial F}{\partial \sigma} \right]_0 = 0, \quad (82)$$

$$\left. \frac{\partial G}{\partial \rho} \right]_0 = -uA, \quad (83)$$

$$\left. \frac{\partial G}{\partial \sigma} \right]_0 = 1 - \frac{1}{\tau}, \quad (84)$$

which is the same result of Eqs. (56-59). This matrix has two eigenvalues:  $1 - 1/\tau$  and  $A$ . The eigenvalue  $1 - 1/\tau$  corresponds to the  $\sigma$  axis, which is a

stable direction. The eigenvalue  $A$  corresponds to a unstable (stable) direction for  $A > 1$  ( $A < 1$ ).

If we assume that we are close to criticality, where  $\rho^*$  is small, we can find an approximate solution for  $J(\rho, \sigma)$  at the nontrivial fixed point. Expanding the binomial in equation (26) to first order and solving for  $\rho^*$ , we find:

$$\rho^* = \frac{A-1}{A+u\tau}, \quad (85)$$

$$\sigma^* = \frac{A+u\tau}{1+u\tau} = 1 + \frac{A-1}{1+u\tau}, \quad (86)$$

where we used equation (29) to compute  $\sigma^*$ . Note that, as before, this solution exists only if  $A-1 > 0$ . This is the exact condition to the absorbing state solution be unstable.

Inserting in equations (76-79), we have:

$$J = \begin{pmatrix} 1-a & b \\ -c & 1-d \end{pmatrix}, \quad (87)$$

where

$$a = \frac{(2K-1)(A-1)}{K(1+u\tau)}, \quad (88)$$

$$b = \frac{A-1}{(A+u\tau)^2} \left( 1+u\tau - \frac{(A-1)(K-1)}{K} \right), \quad (89)$$

$$c = \frac{u(A+u\tau)}{1+u\tau}, \quad (90)$$

$$d = \frac{1}{\tau} + \frac{u(A-1)}{A+u\tau}. \quad (91)$$

Note that they are all positive quantities. The eigenvalues of  $J$  are:

$$\lambda^\pm = 1 - \frac{a+d}{2} \pm \frac{1}{2} \sqrt{(a-d)^2 - 4bc}. \quad (92)$$

For systems to be close to criticality, we must have  $\tau \gg 1$ . Thus,  $a$ ,  $b$  and  $d$  are of  $O(1/\tau)$ , while  $c = O(1)$ . Therefore, the  $4bc$  term dominates the square root argument in equation (92). Hence, we have two complex conjugate eigenvalues with modulus and argument given by:

$$|\lambda^\pm| = \sqrt{1 - (a+d) + da + bc}. \quad (93)$$

We can expand  $|\lambda^\pm|$  in powers of  $1/\tau$ :

$$|\lambda^\pm| = 1 - \left( \frac{(A-1)(2K-1)}{2uK} + \frac{1}{2} \right) \frac{1}{\tau} + O(\tau^{-2}). \quad (94)$$

This confirms that the same scenario of barely stable spirals appears in the CA model. The harmonic frequency is:

$$\omega \equiv |\omega^\pm| = \arctan \frac{\sqrt{4bc - (a-d)^2}}{2 - (a+d)}. \quad (95)$$

To first order in  $\tau$ , we get:

$$\omega \simeq \sqrt{\frac{A-1}{\tau}} \quad (96)$$

which shows that the frequency of oscillations is vanishingly small for large  $\tau$ , being identical to equation (73).